IEEE Photonics Journal
An IEEE Photonics Society Publication

Open Access

Stokes Space Modulation Format Identification for Optical Signals Using Probabilistic Neural Network

Volume 10, Number 3, June 2018

Ming Hao
Lianshan Yan
Anlin Yi
Lin Jiang
Yan Pan
Wei Pan
Bin Luo

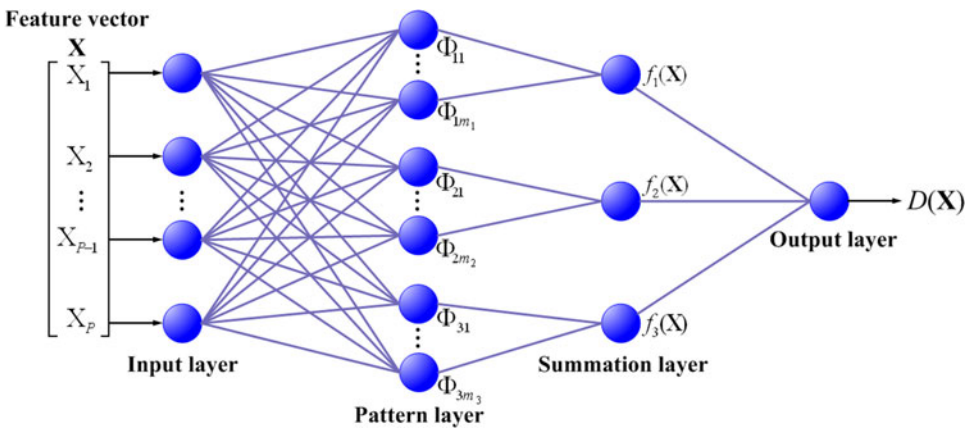

DOI: 10.1109/JPHOT.2018.2836151
1943-0655 © 2018 IEEE

Stokes Space Modulation Format Identification for Optical Signals Using Probabilistic Neural Network

Ming Hao,[1,2] **Lianshan Yan**,[1] **Anlin Yi**,[1] **Lin Jiang**,[1] **Yan Pan**,[1] **Wei Pan**,[1] **and Bin Luo**[1]

[1]Center for Information Photonics and Communications, School of Information Science and Technology, Southwest Jiaotong University, Chengdu 611756, China
[2]School of Automation and Information Engineering, Sichuan University of Science and Engineering, Zigong 643000, China

DOI:10.1109/JPHOT.2018.2836151

Manuscript received April 4, 2018; revised May 5, 2018; accepted May 9, 2018. Date of publication May 14, 2018; date of current version June 1, 2018. This work was supported in part by the National Natural Science Foundation of China under Grants 61335005, 61325023, and 61401378, and in part by the Artificial Intelligence Key Laboratory of Sichuan Province under Grant 2016RYJ05. Corresponding author: Lianshan Yan (e-mail: lsyan@home.swjtu.edu.cn).

Abstract: A Stokes space modulation format identification (MFI) method using probabilistic neural network (PNN) is proposed for coherent optical receivers. According to amplitude histograms obtained by the distribution of Stokes vectors on the s_1 axis, the incoming signals are first classified into PDM-*m*PSK, PDM-16QAM, and PDM-64 QAM signals based on PNN. To further identify PDM-*m*PSK signals, the constellation feature of Stokes vectors on s_2–s_3 plane is extracted by image processing techniques and then processed by PNN. The high identification accuracy is demonstrated via numerical simulations with 28-Gbaud PDM-QPSK, PDM-8PSK, PDM-16QAM, and PDM-64QAM signals over a wide optical signal-to-noise ratio range. Owing to the characteristic of PNN, the proposed MFI method has simple training process, small training data size and a small number of required symbols. Proof-of-concept experiments have been implemented to verify the effectiveness of the proposed MFI method among 28-Gbaud PDM-QPSK, PDM-8PSK, and PDM-16QAM signals.

Index Terms: Modulation format identification, coherent optical communications, probabilistic neural network.

1. Introduction

In order to meet the demands for ever-growing emerging services such as internet of things, streaming video, big data, cloud computing and so on, the next generation optical networks require higher spectral efficiency and more dynamic flexibility [1]. Thus the elastic optical networks (EONs) [2] which are efficient, programmable and flexible have recently aroused much research interests. The key element of EON is the variable transponder which allows adaptive data rate and modulation format based on channel state information to support emerging services. Therefore, the coherent optical receivers in EONs need to identify the modulation format of the received signals autonomously. Correct modulation format can ensure modulation format dependent algorithms that embedded in the digital signal processing (DSP) module to obtain optimal performance.

In recent years, DSP algorithms have been widely employed to implement modulation format identification (MFI) in fiber-optic networks. These include: (i) received signal power distributions

based method [3], which demands prior information about optical signal-to-noise ratio (OSNR) of the received optical signal; (ii) artificial neural network (ANN) based method [4], which employs asynchronous amplitude histograms of directly detected signals; (iii) methods based on *K*-means algorithm [5] and convolution neural network (CNN) [6], which demand constellation diagram obtained at the final stage of the DSP chain; (iv) deep neural network (DNN) based method [7], which requires considerable computational resources as well as processing time to complete the training process; (v) peak-to-average-power ratio (PAPR) based method [8], which needs to establish different thresholds under each OSNR value; (vi) support vector machine (SVM) based method [9], which employs features of power eyediagram of directly detected signals; (vii) cumulative distribution function (CDF) based method [10], which identifies modulation formats by using the normalized amplitudes of signals so that it is not applicable to identifying *m*PSK modulation formats; (viii) nonlinear power transformation based method [11], which would require longer fast Fourier transform (FFT) for higher-order QAM signals to cope with reduction of PAPR caused by imperfect symbol partitioning; (ix) Godard's error based method [12], which utilizes the intensity fluctuation feature after pre-equalization to identify modulation formats; (x) Stokes space based methods [13]–[17], which applied in early stage of the DSP chain. Among these methods, Stokes space based methods have attracted significant attentions because they are insensitive to carrier phase noise, frequency offset and polarization mixing. Furthermore, Stokes space based methods can be applied before modulation format dependent algorithms including polarization demultiplexing [18], frequency offset compensation as well as carrier phase recovery, and could ensure optimal system performance.

In this paper, we present a Stokes space MFI method based on probabilistic neural network (PNN) for coherent optical receivers. In which, PNN is a kind of feed-forward artificial neural network [19], which can approach a Bayes-optimal solution [20], and has been found suitable for pattern recognition and classification [21], [22]. According to amplitude histograms obtained by the distribution of Stokes vectors on the s_1 axis, the incoming polarization-division multiplexing (PDM) signals are firstly classified into PDM-*m*PSK, PDM-16QAM and PDM-64QAM signals based on PNN. To further identify PDM-*m*PSK signals, the constellation feature of Stokes vectors on s_2–s_3 plane is extracted by image processing techniques and then processed by PNN. The high identification accuracy of the proposed MFI method is demonstrated via numerical simulations with 28-Gbaud PDM-QPSK, PDM-8PSK, PDM-16QAM and PDM-64QAM signals over a wide OSNR range. Furthermore, the effectiveness is verified by proof-of-concept experiments among 28-Gbaud PDM-QPSK, PDM-8PSK and PDM-16QAM signals. Without any iteration and back-propagation for adjusting parameters [23], the training process of PNN is simple. Meanwhile, the proposed MFI method is non-data-aided (NDA). Simulation and experiment results show that the proposed method requires small training data size and a small number of required symbols.

2. Operating Principle

The DSP architecture with proposed MFI method for coherent optical receivers is shown in Fig. 1. The proposed MFI method, as shown in the red box, is placed behind the modulation format independent algorithms that comprise chromatic dispersion (CD) compensation and timing phase recovery algorithms. Modulation format information obtained by the proposed MFI method is provided to the subsequent modulation format dependent algorithms that composed of polarization demultiplexing, frequency offset compensation and carrier phase recovery to guarantee optimal system performance.

As shown in Fig. 1, the proposed MFI method consists of three steps. Power normalization and Stokes space mapping is necessary before MFI to transform the received signals into Stokes space. In addition, random rotation of the state of polarization (SOP) occurs due to random perturbation, thus SOP tracking and correction is required to guarantee the optimal performance of MFI. It should be noted that the procedure of SOP tracking and correction in Stokes space is much easier than that in the Jones space, and is modulation format independent [16], [17]. Moreover, the calculated polarization rotation matrix in the SOP tracking and correction process can then be used for subsequent polarization demultiplexing algorithm such as CMA equalization to significantly

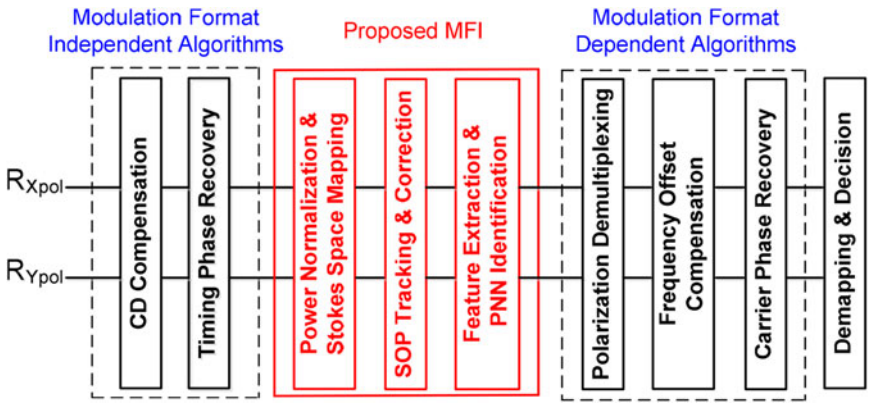

Fig. 1. DSP architecture with proposed MFI method for coherent optical receivers.

improve the convergence speed [24], [25]. Finally, based on the extracted feature of Stokes vectors, PNN realizes identification of four commonly used modulation formats including PDM-QPSK, PDM-8PSK, PDM-16QAM and PDM-64QAM.

2.1 Stokes Mapping and SOP Correction

The received PDM signals (i.e., one sample per symbol) e_x and e_y can be transformed into Stokes space after CD compensation, timing phase recovery and power normalization, and expressed as [26]

$$S = \begin{bmatrix} s_0 \\ s_1 \\ s_2 \\ s_3 \end{bmatrix} = \begin{bmatrix} e_x e_x^* + e_y e_y^* \\ e_x e_x^* - e_y e_y^* \\ e_x^* e_y + e_x e_y^* \\ -j e_x^* e_y + j e_x e_y^* \end{bmatrix} = \begin{bmatrix} a_x^2 + a_y^2 \\ a_x^2 - a_y^2 \\ 2a_x a_y \cos\Delta\theta \\ 2a_x a_y \sin\Delta\theta \end{bmatrix} \tag{1}$$

where, a_x and a_y are the magnitudes of the received two PDM signals, respectively. $\Delta\theta$ denotes the phase difference between the two signals. s_0 represents the total power, while the last three components of the Stokes vector, $[s_1,\ s_2,\ s_3]^{\mathrm{T}}$, indicate SOP of the received PDM signals.

The received PDM signals present a lens-like object in stokes space. The existence of the lens-like object in Stokes space uniquely identifies a symmetry plane and its normal $\mathbf{n}$ ($[n_1,\ n_2,\ n_3]^{\mathrm{T}}$). The symmetry plane can be found from a least squares fit of stokes vectors [26]. In order to realize MFI, the rotated SOP due to random perturbation needs to be corrected and then features of various modulation formats can be extracted more accurately. Therefore, the normal $\mathbf{n}$ ($[n_1,\ n_2,\ n_3]^{\mathrm{T}}$) of the arbitrary least squares plane (LSP) should be aligned to the direction of the s_1 vector (i.e., the normal of the standard LSP) in Poincare sphere, whose value is $[\,1, 0, 0\,]^{\mathrm{T}}$. The SOP tracking and correction can be implemented by using inverse transformation matrix which is defined as [27]

$$M^{-1} = \begin{pmatrix} \cos(\alpha)\exp(j\Delta\phi/2) & \sin(\alpha)\exp(-j\Delta\phi/2) \\ -\sin(\alpha)\exp(j\Delta\phi/2) & \cos(\alpha)\exp(-j\Delta\phi/2) \end{pmatrix} \tag{2}$$

where $\alpha = 2^{-1}\arctan\left(n_1, \sqrt{n_2^2 + n_3^2}\right)$ and $\Delta\phi = \arctan(n_2, n_3)$. By employing (2), SOP tracking and correction can be realized in Stokes space.

2.2 Feature Extraction of Modulation Formats

As well known, different PDM modulation formats, such as PDM-QPSK, PDM-8PSK, PDM-16QAM and PDM-64QAM, have different features in three-dimensional (3D) Stokes space. The four commonly used PDM modulation formats in Stokes space have different numbers of clusters as shown

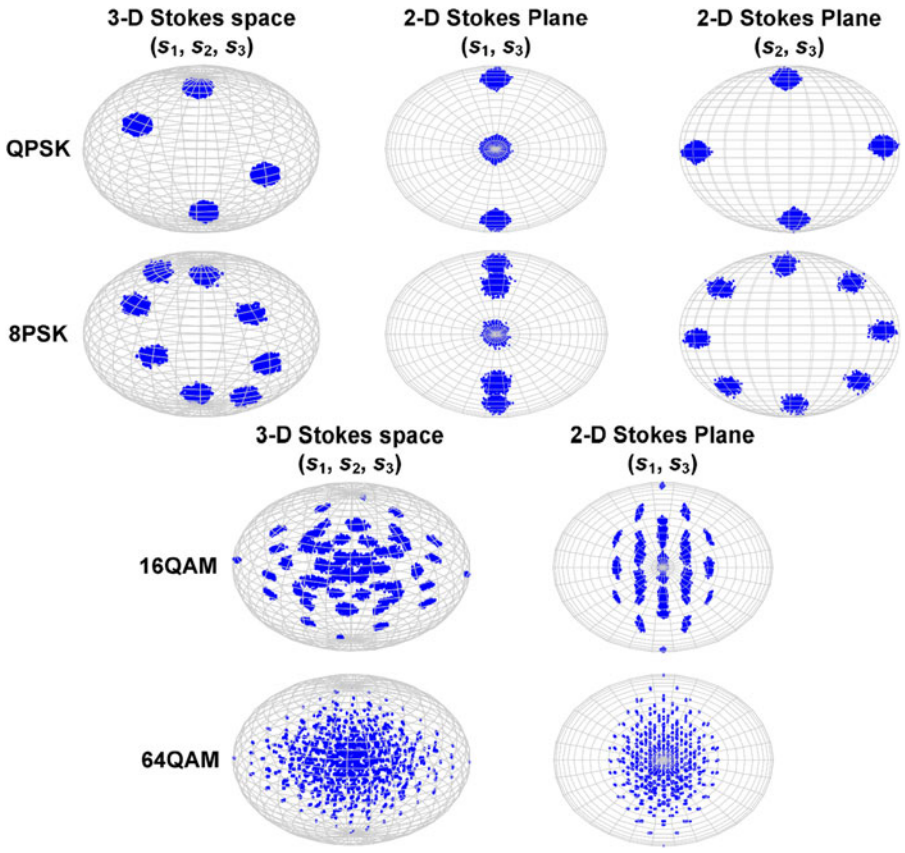

Fig. 2. Ideal Stokes representation in Poincaré sphere of four commonly used PDM modulation formats.

in Fig. 2. However, it is difficult to identify the 3D clusters in practical system especially for high-order modulation formats which have a large number of clusters.

Meanwhile, PDM-*m*PSK, PDM-16QAM and PDM-64QAM signals have different distributions of Stokes vectors on the s_1 axis. For PDM-*m*PSK signal, there is only one level on the s_1 axis due to its constant amplitude, and s_1 can be expressed as

$$s_1 = a_x^2 - a_y^2 = 0 \tag{3}$$

Unlike PDM-*m*PSK signal, the amplitudes of high-order QAM signal are not constant. For PDM-16QAM signal, the amplitudes of constellation points are $\sqrt{2}$, $\sqrt{10}$ and $3\sqrt{2}$, respectively. Therefore, there are five levels on the s_1 axis, and s_1 can be calculated as

$$s_1 = a_x^2 - a_y^2 = -16, -8, \ 0, \ 8, \ 16 \tag{4}$$

Similar to PDM-16QAM, PDM-64QAM signal have multi-levels on the s_1 axis. The amplitudes of constellation points are $\sqrt{2}$, $\sqrt{10}$, $3\sqrt{2}$, $\sqrt{26}$, $\sqrt{34}$, $5\sqrt{2}$, $\sqrt{58}$, $\sqrt{74}$ and $7\sqrt{2}$, thus there are twenty-five levels on the s_1 axis. The levels of different modulation formats can be clearly seen on the 2D Stokes plane (s_1, s_3) of Fig. 2.

Since PDM-*m*PSK signals have same feature on the s_1 axis, the relative phase information $\Delta\phi$ on 2D Stokes plane (s_2, s_3) is employed to further distinguish PDM-QPSK and PDM-8PSK signals, and can be defined as

$$\Delta\phi = \phi_x - \phi_y = (\omega_\Delta t + \theta_{sx} + \theta_n) - (\omega_\Delta t + \theta_{sy} + \theta_n) = \theta_{sx} - \theta_{sy} \tag{5}$$

where ω_Δ indicates frequency offset between the transmitting laser and the receiving local oscillator (LO) laser. θ_{sx} and θ_{sy} denote the modulation format phase information of the received X and Y

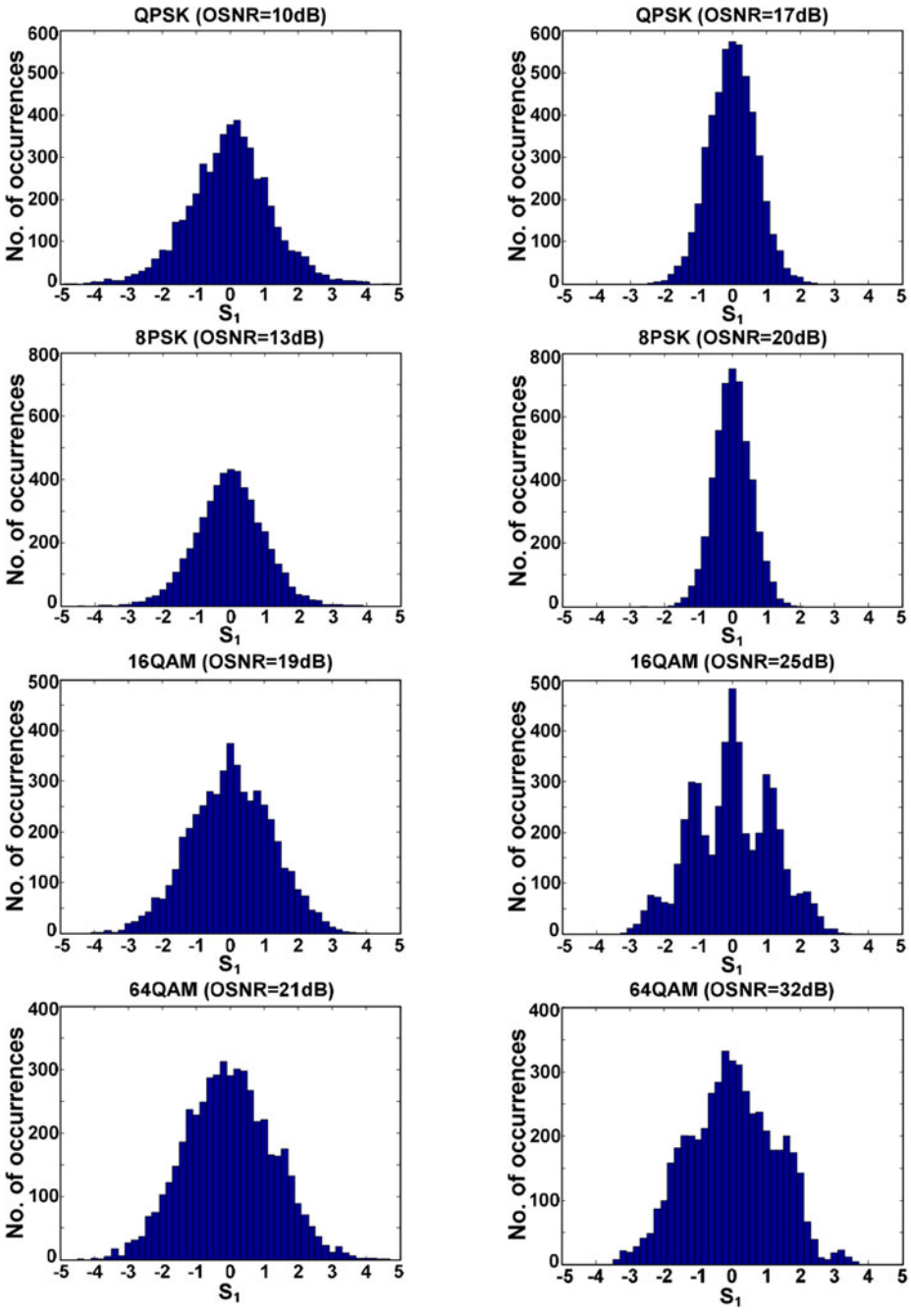

Fig. 3. Amplitude histograms on the s_1 axis of four commonly used PDM modulation formats.

polarization signals, respectively. θ_n is the laser phase noise. Since the phase information of PDM-QPSK signal are $-3\pi/4$, $-\pi/4$, $\pi/4$, and $3\pi/4$, the relative phase information $\Delta\phi$ are 0, $\pi/2$, π, and $3\pi/2$, respectively. Thus 4 clusters would appear on Stokes plane (s_2, s_3). Similarly, for PDM-8PSK, the number of clusters presented on Stokes plane (s_2, s_3) is 8. The distributions of clusters of PDM-QPSK and PDM-8PSK signals on Stokes plane (s_2, s_3) are shown in Fig. 2.

The amplitude histograms on the s_1 axis of the four commonly used PDM modulation formats are shown in Fig. 3. It should be noted that, in order to maintain satisfactory discrimination, the three components of the Stokes vector $[s_1, s_2, s_3]^T$ in the proposed MFI method are not normalized

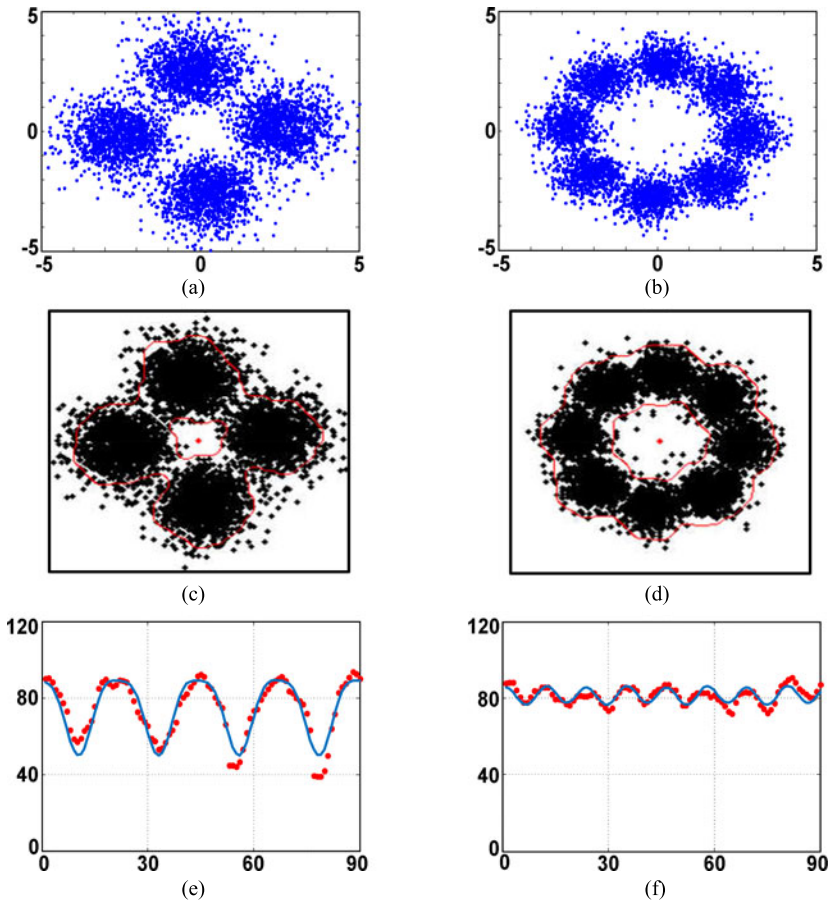

Fig. 4. Constellations on Stokes plane (s_2, s_3) of (a) PDM-QPSK and (b) PDM-8PSK; their converted binary graph with envelope of (c)–(d); their corresponding amplitude of outer envelope with Fourier fitting of (e)–(f).

by max (s_0). Only power normalization is applied before Stokes space mapping, thus the range of feature extraction is set to $[-5, 5]$ on the s_1 axis. As shown in Fig. 3, the amplitude histograms (i.e., 51 bins) of PDM-QPSK, PDM-8PSK, PDM-16QAM, and PDM-64QAM signals have their own features, especially in high OSNR case. The distributions of PDM-QPSK and PDM-8PSK signals concentrate around 0 on the s_1 axis when the OSNR is high. However, the distribution is broadened due to noise in low OSNR case. For PDM-16QAM signal, the five levels are much more apparent when the OSNR is 25 dB compared to 19 dB case. Since there are twenty-five levels for PDM-64QAM signal on the s_1 axis, the levels are not obvious even the OSNR rises to 32 dB. Owing to powerful performance of PNN, PDM-64QAM signals also can be identified even in relative low OSNR case. If the number of symbols used for MFI is not sufficient, the levels close to the edge are not evident. Thus, 5000 symbols are used in Fig. 3 to exhibit the distribution more apparently.

The constellations on Stokes plane (s_2, s_3) of PDM-QPSK and PDM-8PSK are shown in Fig. 4(a) and (b), respectively. The number of symbols is 5000, while the OSNR of PDM-QPSK and PDM-8PSK signals are 16 dB and 21 dB, respectively. As mentioned above, PDM-QPSK signal can be distinguished from PDM-8PSK signal based on the number of clusters on Stokes plane (s_2, s_3), and different numbers of clusters would certainly lead to distinguishable outer envelope. Therefore, image processing techniques is employed to obtain the outer envelope of these two modulation formats. Firstly, the constellation on Stokes plane (s_2, s_3) is converted into binary graph with size of $221 * 221$ pixels. The converted binary graphs for PDM-QPSK and PDM-8PSK signals are shown in Fig. 4(c) and (d), respectively. Here, morphological opening [28] based on erosion and

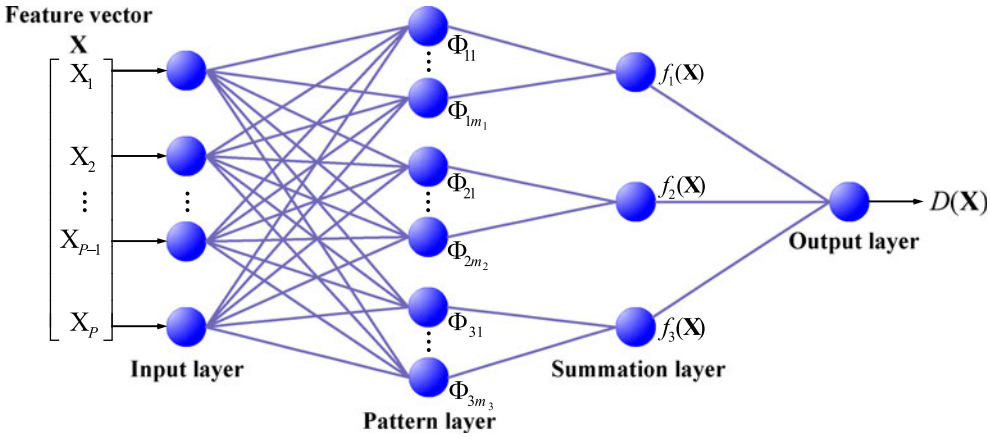

Fig. 5. Schematic diagram of PNN.

dilation operations is used to remove the deviation points. After deviation points are removed, edge detection is implemented by Sobel method. The Sobel method utilizes two vertical and horizontal operators to do convolution on the binary graph and then obtain the edge intensity [29]. Based on edge intensity, the envelope of constellations can be obtained. The red lines in Fig. 4(c) and (d) are envelope of constellations and the red points in the center are the origin of Stokes plane (s_2, s_3). As the edge extraction is accomplished, the amplitude of outer envelope per 4 degree in phase (i.e., 4 degree $\times$ 90 $=$ 360 degree) is obtained. The outer envelope of PDM-QPSK signal presents 4 distinct peaks due to 4 clusters. On the contrast, eight smooth peaks appear on the outer envelope of PDM-8PSK signal because of 8 clusters. In order to reduce fluctuation caused by noise, Fourier fitting [30] which fit the amplitude of outer envelope in the form of 2-order Fourier series is employed. The amplitudes of outer envelope utilizing Fourier fitting for PDM-QPSK and PDM-8PSK signals are shown in Fig. 4(e) and (f), respectively. To reduce the complexity of PNN, only 45 points are extracted in the fitting curve. Furthermore, each extracted point is weighted by the average value of the 45 extracted points for better separation of the features between PDM-QPSK and PDM-8PSK signals.

2.3 PNN Identification

Since carrying out decision classification based on posterior probability, Bayesian decision theory can minimize the expected risk and is applicable to multi-classification problems [19]. Based on Bayesian decision theory, PNN can process data sets which are incomplete or deteriorated by noise in pattern classification tasks. In this paper, PNN is employed to realize MFI based on the amplitude histograms of Stokes vectors on the s_1 axis and the constellation features of Stokes vectors on s_2-s_3 plane.

As shown in Fig. 5, The PNN comprises input layer, pattern layer, summation layer and output layer. The first layer is input layer which transfers feature vector $\mathbf{X}$ of testing modulation format sample to all neurons of pattern layer. The neuron number of input layer is determined by the dimensionality p of feature vector. Subsequently, pattern layer calculates the matching relation between the feature vector $\mathbf{X}$ of testing modulation format sample and the feature vector $\mathbf{X}_{nk}$ of training modulation format sample (i.e., $k = 1, \ldots, m_n$. m_n is the total number of training samples for n-th modulation format). Each training modulation format sample corresponds to a single neuron. Therefore, the neurons in the pattern layer depend on the sum of all modulation format samples in the training set. The output of each neuron in pattern layer can be expressed as

$$\Phi_{nk}(\mathbf{X}) = \frac{1}{(2\pi)^{p/2}\sigma^p} \exp\left[-\frac{(\mathbf{X}-\mathbf{X}_{nk})^T(\mathbf{X}-\mathbf{X}_{nk})}{2\sigma^2}\right] \tag{6}$$

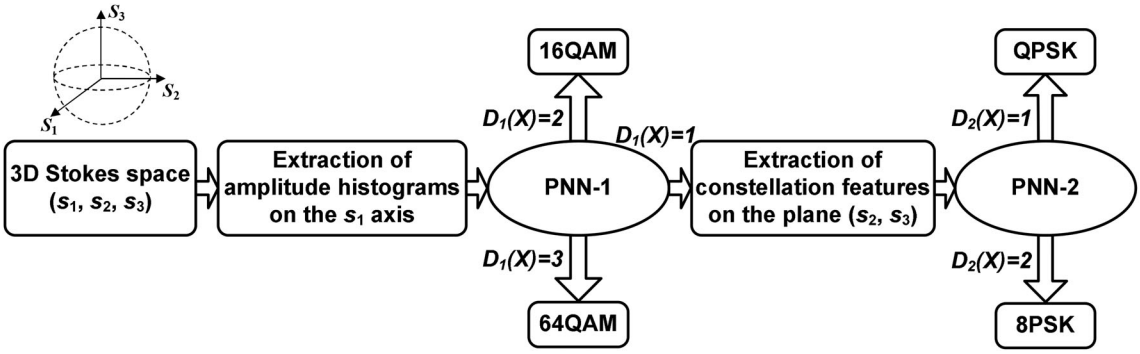

Fig. 6. Flow chart for the proposed MFI method.

where σ denotes the smoothing parameter and $(\cdot)^T$ represents transpose operation. Next, the summation layer needs to implement summarizing and averaging among the neurons belonging to the same class in the pattern layer. The output of each neuron in summation layer can be calculated as

$$f_n(\mathbf{X}) = \frac{1}{m_n} \sum_{k=1}^{m_n} \Phi_{nk}(\mathbf{X}) \tag{7}$$

The last layer is output layer which determines the class of testing modulation format sample by (8).

$$D(\mathbf{X}) = \arg \max \left\{ f_n(\mathbf{X}) \right\}, \; n = 1, \; 2, \; \ldots, \; N \tag{8}$$

where $D(\mathbf{X})$ represents the estimated class label of $\mathbf{X}$, and N denotes the total number of the modulation format classifications.

As mentioned above, the network structure of PNN is determined easily by the dimensionality of feature vector, the sum of all training modulation format samples, and the classification of modulation formats, without any complicated process to ascertain the numbers of hidden layers and neurons. Furthermore, the most important advantage of PNN is that training is easy and instantaneous [19]. Without any iteration and back-propagation for adjusting parameter, only one-step weight assignment is needed [23], thus the training process of PNN is simple and fast. The neurons of pattern layer are assigned directly by feature vectors of training modulation format samples. After assignment, the neurons of PNN will never be altered unless increasing new training modulation format samples. Therefore, the training time is just slightly longer than data reading time. Even in increasing new training modulation format samples case, it doesn't require long time training again, but only assigns the corresponding new neurons in pattern layer. Running procedure of PNN is implemented by matrix manipulation, and can converge to Bayes-optimal solution with high stability.

The flow chart for the proposed MFI method is shown as Fig. 6. Based on amplitude histograms on the s_1 axis, PDM-mPSK, PDM-16QAM and PDM-64QAM signals can be identified by PNN-1, and the output $D_1(\mathbf{X})$ of PNN-1 is 1, 2 or 3. If the modulation format is identified as PDM-mPSK (i.e., $D_1(\mathbf{X}) = 1$), further MFI process is needed, otherwise the MFI process is finished. Subsequently, the second PNN is applied based on the extraction of constellation features on the Stokes plane (s_2, s_3). Then, the estimated modulation format type is obtain based on the output $D_2(\mathbf{X})$ (i.e., $D_2(\mathbf{X}) = 1$ for PDM-QPSK or $D_2(\mathbf{X}) = 2$ for PDM-8PSK).

3. Simulation Analysis

In order to verify the feasibility of proposed method, numerical simulation has been employed based on the commercial VPI Transmission Maker. In the transmission system, 28-Gbaud PDM-QPSK,

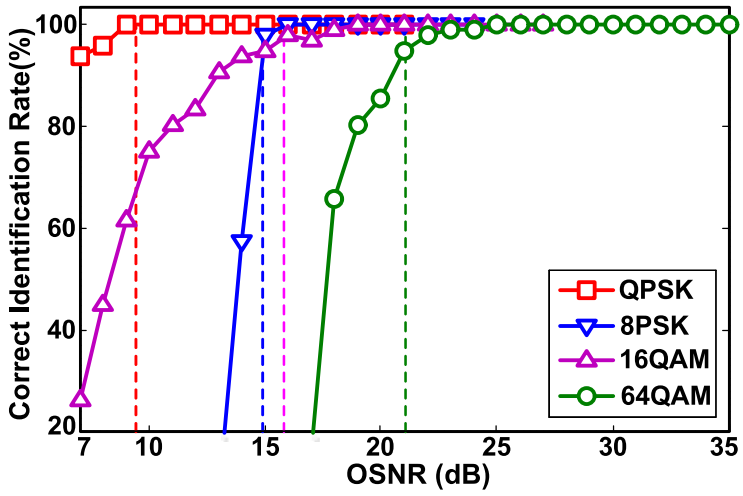

Fig. 7. Simulation results of correct identification rate under different OSNR values.

PDM-8PSK, PDM-16QAM, and PDM-64QAM signals are generated and passed through an additive Gaussian white noise channel with variable OSNR. MFI is implemented by off-line DSP module as shown in Fig. 1. One sample of each OSNR value of each modulation format is regarded as training sample, while ninety-six samples are employed to validate correct identification rate for each OSNR value. However, it should be noted that the modulation format sample extracted in excessive low OSNR case can't be used as training sample since in such case the feature is indistinct owing to the influence of noise. When the samples extracted in excessive low OSNR case are added into training set, the identification performance would be degraded since PNN requires representativeness of the training samples. Therefore, the training set of PNN-1 is consists of thirty-four training samples generated from PDM-QPSK (i.e., 10∼16 dB OSNR), PDM-8PSK (i.e., 17∼23 dB OSNR), PDM-16QAM (i.e., 19∼27 dB OSNR), and PDM-64QAM (i.e., 25∼35 dB OSNR). PNN-2 is employed to further identify PDM-*m*PSK signals. Since the constellation feature of PDM-QPSK is obvious when OSNR is high, there's no need to generate training sample of each high OSNR value. Therefore, eight training samples are generated from 10∼13 dB, 15 dB, 17 dB, 19 dB, and 21 dB OSNR for PDM-QPSK. Meanwhile, eight samples which generated from 17∼24 dB OSNR range are used to be training samples for PDM-8PSK. In our proposed method, the total number of samples in the training set is less than that of the existing MFI methods based on other neural networks [6], [7].

To evaluate the performance of the proposed MFI method, simulation results of correct identification rate under different OSNR values are shown in Fig. 7. Here, 5000 symbols are used to extract features (i.e., 51 amplitude histogram bins or 45 constellation feature points) for each training and testing modulation format sample. Specifically, the minimum required OSNR to achieve correct identification rate higher than 95% is used as a metric to evaluate the identification performance [15], [17], [31]. As shown in Fig. 7, the proposed MFI method can achieve 95% correct identification rates when the OSNR values of each modulation format are higher than the thresholds (vertical dash lines) corresponding to 20% FEC correcting bit error rate (BER) of 2.4e-2.

To comprehensively evaluate the performance, we compare our proposed method with Stokes space method based on the non-iterative density-peak-search clustering algorithm [17]. The minimum required OSNR values for identifying the different modulation formats (i.e., PDM-QPSK, PDM-16QAM, PDM-64QAM) with the two methods are shown in Fig. 8. In our proposed method, the minimum required OSNR values for PDM-QPSK, PDM-16QAM and PDM-64QAM signals are 8 dB, 16 dB and 22 dB, respectively. These are lower than or equal to the minimum required OSNR values of method in [17]. Furthermore, in order to achieve successful identification, the proposed method requires 5000 symbols for each modulation format sample, while 8000 symbols are needed

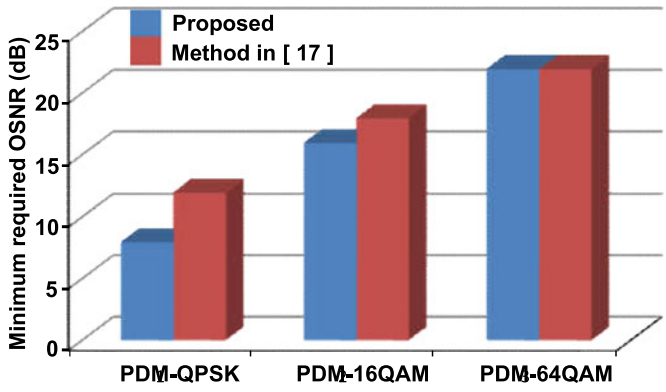

Fig. 8. The minimum required OSNR for identifying the different modulation formats (i.e., PDM-QPSK, PDM-16QAM, PDM-64QAM) with two identification methods.

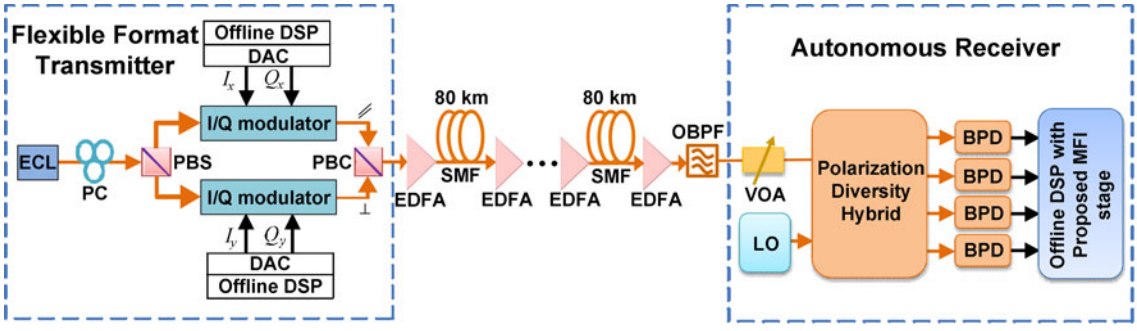

Fig. 9. Experimental setup of EON. PC: polarization controller; PBS: polarization beam splitter; PBC: polarization beam combiner; VOA: variable optical attenuator.

for PDM-64QAM in [17]. In realistic modulation format identification, the required number of symbols is determined by the maximum value of all identified modulation formats.

4. Experimental Verifications

In order to further verify feasibility of our proposal, a proof-of-concept experiment in EON with flexible format transmitter and autonomous receiver has been performed. Different modulation formats based on the transmission capacity can be exported by flexible format transmitter, and identified by autonomous receiver. The experimental setup is shown in Fig. 9. At the transmitter side, a word length of $2^{15} - 1$ pseudo-random bit sequence (PRBS) is generated, and needs to map into modulation format with 2 samples/ symbol. The up-sampled signals are shaped by using a square root raised cosine (SRRC) with a roll-off factor of 1.0. Next, a pre-distortion operation is utilized to overcome the frequency roll-off of a digital to analog converter (DAC). The light from an external cavity laser (ECL) at ~1550-nm with ~100-kHz linewidth is modulated by an integrated $LiNbO_3$ polarization-multiplexing I/Q modulator. The four branches of the modulator are driven by the DAC operating at 64-GSa/s and 25-GHz analog bandwidth for obtaining 28-Gbaud PDM-QPSK, PDM-8PSK, PDM-16QAM signals. The transmission optical link is composed of multi-spans single-mode fiber (SMF) whose dispersion parameter, attenuation, and nonlinear coefficient are $D = 16.9$ ps/nm/km, $a = 0.2$ dB/km, $g = 1.27$ km^{-1}•W^{-1}, respectively. Fiber loss of each span is completely compensated using an erbium doped fiber amplifier (EDFA) with a noise figure of ~5 dB. An optical band-pass filter (OBPF) in link is used to filter amplified spontaneous emission (ASE) noise. After passing though transmission link, the modulated optical signal are combined with LO at the polarization diversity hybrid, and then photo detected by the balanced photo-detector

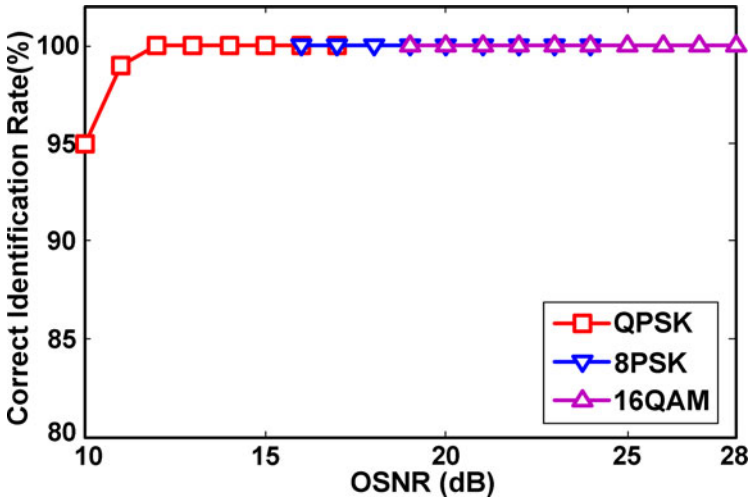

Fig. 10. Results of correct identification rate under different OSNR values in back-to-back experiments.

(BPD). Finally, the electrical signals are processed by off-line DSP module where the proposed MFI method embedded.

At first, the results of correct identification rate under different OSNR values are calculated in back-to-back experiments. For each measured OSNR value (i.e., 10∼17 dB for PDM-QPSK signal, 16∼24 dB for PDM-8PSK signal, and 19∼28 dB for PDM-16QAM signal), 100 independent testing modulation format samples are applied to validate correct identification rate. In common with simulation, training and testing modulation format samples are obtained by 5000 symbols. Here, PDM-QPSK, PDM-8PSK and PDM-16QAM signals need to be identified, thus the numbers of training modulation format samples are twenty-four and sixteen for PNN-1 and PNN-2, respectively. As shown in Fig. 10, the proposed MFI method achieves 100% correct identification rates for PDM-8PSK and PDM-16QAM signals over a wide OSNR range. Meanwhile, 100% correct identification rates are also obtained for PDM-QPSK signal when the OSNR values are bigger than or equal to 12 dB. Even if the OSNR value is reduced to 10 dB, the proposed MFI method can still achieve 95% correct identification rate.

The results of correct identification rate under different numbers of symbols in back-to-back experiments are shown in Fig. 11. All the numbers of symbols for modulation format samples including training and testing are changed synchronously. The correct identification rate of PDM-QPSK signal (i.e., OSNR is 11 dB) is still higher than 95% even if the number of symbols is reduced to 2000, and is virtually 100% when the number of symbols is no less than 4500. Meanwhile, 100% correct identification rates are achieved for PDM-8PSK (i.e., OSNR is 16dB) when more than 4000 symbols are applied to extract feature. However, as the number of symbols is less than 2500, constellation feature of Stokes vectors on s_2–s_3 plane is unable to be effectively extracted, so that the correct identification rate declines drastically. PDM-16QAM signal has five levels on the s_1 axis, but PDM-mPSK signals have only one level on the s_1 axis. Thus PDM-16QAM signal has higher tolerance to the change of the number of symbols compared with PDM-mPSK signals. Here, the correct identification rate of PDM-16QAM signal is more than 95% even if the number of symbols is decreased to 1500.

In order to analyze the effect of fiber nonlinearity, transmission experiments for PDM-QPSK (i.e., 2000 km), PDM-8PSK (i.e., 960 km) and PDM-16QAM (i.e., 1040 km) signals have been implemented. The experiment results of correct identification rate under different transmitted power are shown in Fig. 12. The transmitted power range is −3∼6 dBm, and the number of symbols is 5000. The proposed MFI method can virtually achieve 100% correct identification rates for PDM-QPSK, PDM-8PSK and PDM-16QAM signals when the transmitted power range is −2∼6 dBm. As the transmitted power decreases to 3 dBm, the correct identification rates of the three modulation

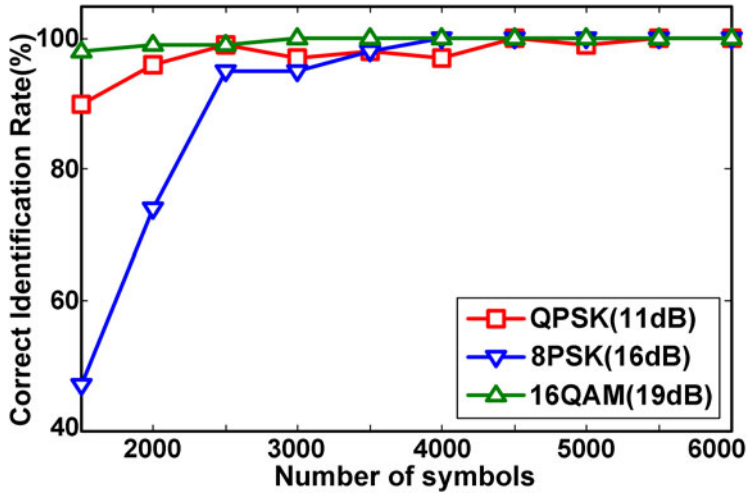

Fig. 11. Results of correct identification rate under different numbers of symbols in back-to-back experiments.

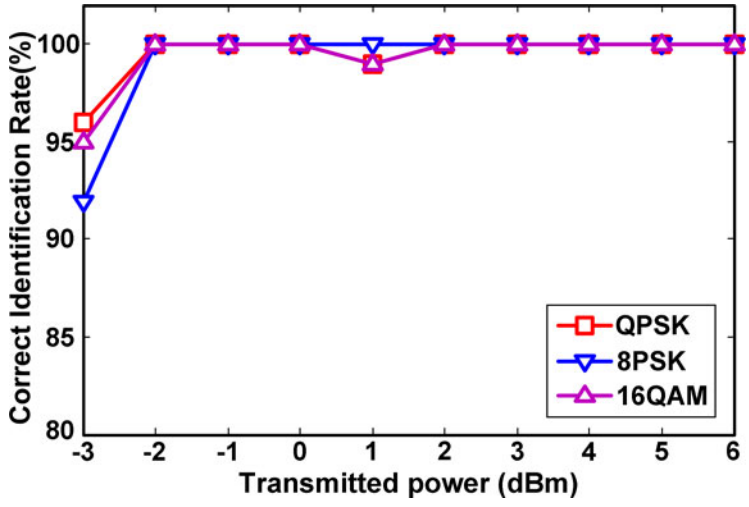

Fig. 12. Experiment results of correct identification rate under different transmitted powers.

formats decline slightly in the presence of noise. The experiment results show that the proposed MFI method is resilient towards fiber nonlinearities.

5. Conclusion

In this paper, a Stokes space MFI method based on PNN is proposed for coherent optical receivers. The high identification accuracy is firstly demonstrated via numerical simulations with 28-Gbaud PDM-QPSK, PDM-8PSK, PDM-16QAM, and PDM-64QAM signals over a wide OSNR range. In addition, proof-of-concept experiments have also been implemented to verify the effectiveness of the proposed MFI method among 28-Gbaud PDM-QPSK, PDM-8PSK and PDM-16QAM signals. Owing to the characteristic of PNN, the proposed MFI method has small training data size and a small number of required symbols. Furthermore, the training process of the proposed MFI method is simple. We believe that our presented method have potential to realize real-time identification of modulation formats in future optical networks.

Reference

[1] L. S. Yan, X. Liu, and W. Shieh, "Toward the Shannon limit of spectral efficiency," *IEEE Photon. J.*, vol. 3, no. 2, pp. 325–330, Apr. 2011.

[2] O. Gerstel, M. Jinno, A. Lord, and S. J. B. Yoo, "Elastic optical networking: A new dawn for the optical layer?," *IEEE Commun. Mag.*, vol. 50, no. 2, pp. s12–s20, Feb. 2012.

[3] J. Liu, Z. H. Dong, K. P. Zhong, A. P. T. Lau, C. Lu, and Y. Z. Lu, "Modulation format identification based on received signal power distributions for digital coherent receivers," in *Proc. Opt. Fiber Commun. Conf. Exhib.*, 2014, San Francisco, CA, USA, paper Th4D.3.

[4] F. N. Khan, Y. Zhou, A. P. T. Lau, and C. Lu, "Modulation format identification in heterogeneous fiber-optic networks using artificial neural networks," *Opt. Exp.*, vol. 20, no. 11, pp. 12422–12431, May 2012.

[5] N. G. Gonzalez, D. Zibar, and I. T. Monroy, "Cognitive digital receiver for burst mode phase modulated radio over fiber links," in *Proc. Eur. Conf. Exhib. Opt. Commun.*, 2010, Torino, Italy, paper P6.11.

[6] D. S. Wang *et al.*, "Intelligent constellation diagram analyzer using convolutional neural network-based deep learning," *Opt. Exp.*, vol. 25, no. 15, pp. 17150–17166, Jul. 2017.

[7] F. N. Khan, K. P. Zhong, W. H. Al-Arashi, C. Y. Yu, C. Lu, and A. P. T. Lau, "Modulation format identification in coherent receivers using deep machine learning," *IEEE Photon. Technol. Lett.*, vol. 28, no. 17, pp. 1886–1889, Sep. 2016.

[8] S. M. Bilal, G. Bosco, Z. H. Dong, A. P. T. Lau, and C. Lu, "Blind modulation format identification for digital coherent receivers," *Opt. Exp.*, vol. 23, no. 20, pp. 26769–26778, Oct. 2015.

[9] J. Thrane, J. Wass, M. Piels, J. C. M. Diniz, R. Jones, and D. Zibar, "Machine learning techniques for optical performance monitoring from directly detected PDM-QAM signals," *J. Lightw. Technol.*, vol. 35, no. 4, pp. 868–875, Feb. 2017.

[10] X. Lin, Y. A. Eldemerdash, O. A. Dobre, S. Zhang, and C. Li, "Modulation classification using received signal's amplitude distribution for coherent receivers," *IEEE Photon. Technol. Lett.*, vol. 29, no. 21, pp. 1872–1875, Nov. 2017.

[11] G. C. Liu, R. Proietti, K. Q. Zhang, H. B. Lu, and S. J. Ben Yoo, "Blind modulation format identification using nonlinear power transformation," *Opt. Exp.*, vol. 25, no. 25, pp. 30895–30904, Dec. 2017.

[12] L. Jiang *et al.*, "Chromatic dispersion, nonlinear parameter, and modulation format monitoring based on Godard's error for coherent optical transmission systems," *IEEE Photon. J.*, vol. 10, no. 1, Feb. 2018, Art. no. 7900512.

[13] P. Y. Chen, J. Liu, X. Wu, K. P. Zhong, and X. F. Mai, "Subtraction-clustering-based modulation format identification in Stokes space," *IEEE Photon. Technol. Lett.*, vol. 29, no. 17, pp. 1439–1442, Sep. 2017.

[14] R. Borkowski, D. Zibar, A. Caballero, V. Arlunno, and I. T. Monroy, "Stokes space-based optical modulation format recognition for digital coherent receivers," *IEEE Photon. Technol. Lett.*, vol. 25, no. 21, pp. 2129–2132, Nov. 2013.

[15] R. Boada, R. Borkowski, and I. T. Monroy, "Clustering algorithms for Stokes space modulation format recognition," *Opt. Exp.*, vol. 23, no. 12, pp. 15521–15531, Jun. 2015.

[16] T. W. Bo, J. Tang, and C.-K. Chan, "Blind modulation format recognition for software-defined optical networks using image processing techniques," in *Proc. Opt. Fiber Commun. Conf. Exhib.*, 2016, Anaheim, CA, USA, paper Th2A.31.

[17] X. F. Mai *et al.*, "Stokes space modulation format classification based on non-iterative clustering algorithm for coherent optical receivers," *Opt. Exp.*, vol. 25, no. 3, pp. 2038–2050, Feb. 2017.

[18] M. Hao *et al.*, "Enhanced frequency-domain fractionally spaced equalization for coherent optical transmission system with colored noise," *Opt. Eng.*, vol. 56, no. 6, Jun. 2017, Art. no. 066116.

[19] D. F. Specht, "Probabilistic neural networks," *Neural Netw.*, vol. 3, no. 1, pp. 109–118, 1990

[20] S. G. Wu, F. S. Bao, E. Y. Xu, Y. X. Wang, Y. F. Chang, and Q. L. Xiang, "A leaf recognition algorithm for plant classification using probabilistic neural network," in *Proc. Int. Symp. Signal Process. Inf. Technol.*, Giza, Egypt, 2007, pp. 11–16.

[21] S. Mishra, C. N. Bhende, and B. K. Panigrahi, "Detection and classification of power quality disturbances using S-transform and probabilistic neural network," *IEEE Trans. Power Del.*, vol. 23, no. 1, pp. 280–287, Jan. 2008.

[22] K. Z. Mao, K. -C. Tan, and W. Ser, "Probabilistic neural-network structure determination for pattern classification," *IEEE Trans. Neural Netw.*, vol. 11, no. 4, pp. 1009–1016, Jul. 2000.

[23] D. R. Nayak, R. Dash, B. Majhi, and V. Prasad, "Automated pathological brain detection system: A fast discrete curvelet transform and probabilistic neural network based approach," *Expert Syst. Appl.*, vol. 88, pp. 152–164, Dec. 2017.

[24] M. Chagnon, M. Osman, X. Xu, Q. Zhuge, and D. V. Plant, "Blind, fast and SOP independent polarization recovery for square dual polarization-MQAM formats and optical coherent receivers," *Opt. Exp.*, vol. 20, no. 25, pp. 27847–27865, Nov. 2012.

[25] Z. M. Yu, X. W. Yi, J. Zhang, M. L. Deng, H. B. Zhang, and K. Qiu, "Modified constant modulus algorithm with polarization demultiplexing in Stokes space in optical coherent receiver," *J. Lightw. Technol.*, vol. 31, no. 19, pp. 3203–3209, Oct. 2013.

[26] B. Szafraniec, B. Nebendahl, and T. Marshall, "Polarization demultiplexing in Stokes space," *Opt. Exp.*, vol. 18, no. 17, pp. 17928–17939, Aug. 2010.

[27] Z. Y. Chen *et al.*, "Use of polarization freedom beyond polarization-division multiplexing to support high-speed and spectral-efficient data transmission," *Light Sci. Appl.*, vol. 6, 2017, Art.no. e16207.

[28] M. H. Chen and P. F. Yan," A multiscaling approach based on morphological filtering," *IEEE Trans. Pattern Anal. Mach. Intell.*, vol. 11, no. 7, pp. 694–700, Jul. 2010.

[29] R. C. Gonzalez and R. E. Woods, "Digital image processing," New York, NY, USA: Addison-Wesley, 1992.

[30] P. Zhou, W. B. Zhang, J. X. Wang, J. Liu, R. X. Su, and X. M. Wang, "Multimode optical fiber surface plasmon resonance signal processing based on the Fourier series fitting," *Plasmonics*, vol. 11, pp. 721–727, 2016.

[31] T. W. Bo, J. Tang, and C. K. Chan, "Modulation format recognition for optical signals using connected component analysis," *IEEE Photon. Technol. Lett.*, vol. 29, no. 1, pp. 11–14, Jan. 2017.